Ocean Engineering 235 (2021) 109366

Contents lists available at ScienceDirect

Ocean Engineering

journal homepage: www.elsevier.com/locate/oceaneng

Convex environmental contours

Arne Bang Huseby [a], Erik Vanem [b,*], Christian Agrell [b], Andreas Hafver [b]

[a] University of Oslo, Norway
[b] DNV, Norway

ARTICLE INFO

Keywords:
Environmental contours
Importance sampling
Discrete mixtures
Smoothing

ABSTRACT

Environmental contours are widely used as a basis for e.g., ship design, especially in early design phases. The traditional approach to such contours is based on the well-known Rosenblatt transformation. Here we focus on convex contours estimated using Monte Carlo methods and establish a rigorous mathematical foundation for such contours. In the present paper we also present an improved simulation procedure based on importance sampling. In particular, we show how this procedure can be extended to cases with omission factors and where the joint distribution of the environmental variables is a discrete mixture. It is well-known that contours constructed using Monte Carlo simulation typically have certain irregularities. In particular, the sets bounded by the estimated contours appear to be convex. However, when the curves are investigated more closely, they include a large number of small loops. In the present paper we provide a precise condition for convexity, and propose a smoothing method which can be used to eliminate the loops. The methods are illustrated by a numerical example.

1. Introduction

Environmental contours are widely used as a basis for e.g., ship design. Such contours are typically used in early design when the strength and failure properties of the object under consideration are not known. An environmental contour describes the tail properties of some relevant environmental variables, and is used as input to the design process. See Haver (1987), Baarholm et al. (2010), Ditlevsen (2002), Moan (2009) and Jonathan et al. (2011). The methodology for constructing environmental contours were introduced by Winterstein et al. (1993) and Haver and Winterstein (2009). The process starts out by constructing a contour for two independent standard normally distributed variables. This contour is then transformed to the environmental space using the inverse Rosenblatt transformation introduced in Rosenblatt (1952). As pointed out in Huseby et al. (2013) the probabilistic properties of the contour is typically not preserved under this transformation. Hence, the resulting contour may need to be adjusted in order to get the desired exceedance probability. Huseby et al. (2013) also presented an alternative approach where environmental contours are constructed using Monte Carlo simulation. For a similar approach to a related problem see Ottesen and Aarstein (2006). Improved methods are found in Huseby et al. (2015a,b).

Contour methods are often used in situations where the environmental variables are the *significant wave height* and the *wave period*. By focussing on the significant wave height the uncertainty in the short-term response is essentially ignored. In Winterstein et al. (1993) it is pointed out that largest response can sometimes be produced in a seastate with less-than-maximum significant wave height. Thus, assuming that the worst case responses are proportional to the significant wave height may result in underestimation of the risk. Winterstein et al. (1993) suggest that the uncertainty in the short-term response can be included by adding a random error term, often referred to as an *omission factor*. Still, modelling such a factor in normal space can be challenging. To avoid explicit inclusion of this factor, Winterstein et al. (1993) argue that the uncertainty alternatively can be accounted for by using an inflated contour.

For Monte Carlo contours it is in principle much easier to take into account the uncertainty in the short-term response by adding a random error term since this can be done directly in the environmental space. When running a full-scale Monte Carlo simulation, adding an extra random variable is straightforward. It should be noted, however, that if more advanced Monte Carlo methods, like e.g., importance sampling, is used, it becomes more difficult to include omission factors. A solution to this issue is presented in Section 4.1.

A challenge with Monte Carlo based methods is that in order to obtain stable results it may be necessary to run a large number of simulations. In Huseby et al. (2015b) this issue was addressed by using rejection sampling. In the present paper we show how this can be improved even further using importance sampling. Even though the resulting contours are fairly precise, a closer examination of the

* Corresponding author.
E-mail address: Erik.Vanem@dnv.com (E. Vanem).

https://doi.org/10.1016/j.oceaneng.2021.109366
Received 26 January 2021; Received in revised form 11 May 2021; Accepted 19 June 2021

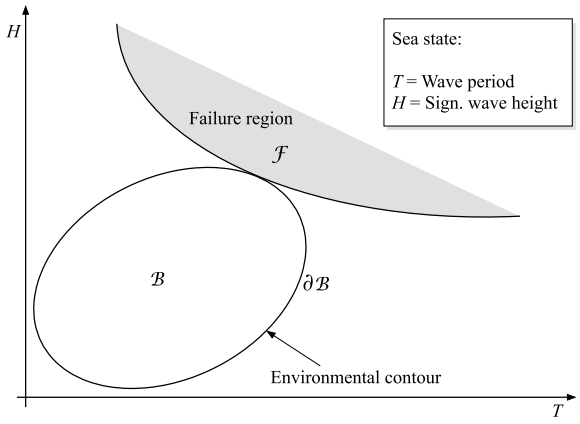

Fig. 2.1. An environmental contour and a failure region.

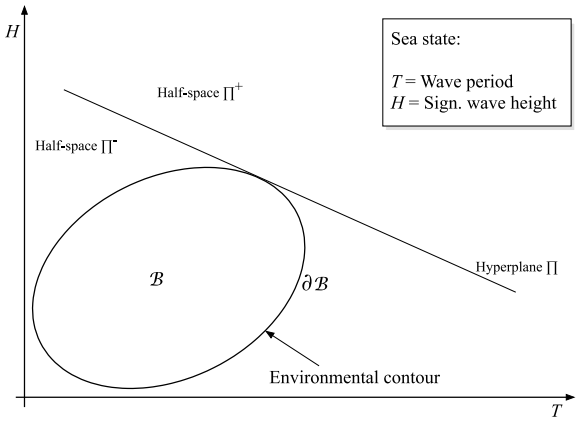

Fig. 3.1. Supporting hyperplane and halfspaces.

curves reveals certain irregularities. In the present paper we study this problem in detail, and show why these irregularities occur. Based on the theoretical results we also propose a simple smoothing method for removing these irregularities.

2. Basic concepts

Let $(T, H) \in \mathbb{R}^2$ be a vector of environmental variables where e.g.,:

T = Wave period

H = Significant wave height

The distribution of (T, H) is assumed to be absolutely continuous with respect to the Lebesgues measure in $\mathbb{R}^2$.

An *environmental contour* is defined as the boundary of a compact[1] set $\mathcal{B} \subseteq \mathbb{R}^2$ and denoted $\partial\mathcal{B}$. To avoid pathological cases we always assume that these sets have a *non-empty* interior. In particular, sets containing just a *single point* will not be considered.

During the design phase of some structure of interest the environmental contour can be used to identify conditions which the structure should be able to withstand. That is, if $(T, H) \in \mathcal{B}$, the structure should function normally. Consequently, the environmental contour $\partial\mathcal{B}$ represents the most severe or extreme conditions that the structure should be able to handle, and the points on this contour represent possible design requirements for the structure.

The *failure region* $\mathcal{F} \subseteq \mathbb{R}^2$ of a structure is the set of states where the structure fails. See Fig. 2.1. For a given environmental contour $\partial\mathcal{B}$ we say that the design requirements are satisfied if and only if the failure region $\mathcal{F}$ does not overlap with the interior of the set $\mathcal{B}$. Formally, we state this as[2] $\mathcal{F} \cap \mathcal{B} \subseteq \partial\mathcal{B}$. That is, the failure region $\mathcal{F}$ is only allowed to intersect with the set $\mathcal{B}$ at its boundary. If the set $\mathcal{B}$ is large, an allowed failure region, $\mathcal{F}$ will be located in the outer regions of the outcome space. This implies that the structure will be subject to strict design requirements. As a result, the probability of failure, i.e., the probability that $(T, H) \in \mathcal{F}$ is small.

In the design phase the exact shape of the failure region of a structure is typically unknown. It may still be possible to argue that the failure region belongs to a certain family denoted by $\mathcal{E}$. We then say that the design requirements are satisfied if and only if $\mathcal{F} \cap \mathcal{B} \subseteq \partial\mathcal{B}$ for all $\mathcal{F} \in \mathcal{E}$.

The *exceedance probability* of $\mathcal{B}$ with respect to $\mathcal{E}$ is defined as:

$$P_e(\mathcal{B}, \mathcal{E}) = \sup_{\mathcal{F} \in \mathcal{E}} \{P[(T, H) \in \mathcal{F}]\}.$$

The exceedance probability is an upper bound on the failure probability of the structure assuming that the true failure region is a member of the family $\mathcal{E}$. For a given target exceedance probability[3] p_e our goal is to find a minimal set $\mathcal{B}$ such that:

$$P_e(\mathcal{B}, \mathcal{E}) \leq p_e. \tag{2.1}$$

If the set $\mathcal{B}$ satisfies (2.1), then $\partial\mathcal{B}$ is said to be a *valid* environmental contour.

A failure region $\mathcal{F} \in \mathcal{E}$ is said to be *maximal* if there does not exist a region $\mathcal{F}' \in \mathcal{E}$ such that $\mathcal{F} \subset \mathcal{F}'$. The family of maximal regions in $\mathcal{E}$ is denoted by $\mathcal{E}^*$. If $\mathcal{F}_1, \mathcal{F}_2 \in \mathcal{E}$ and $\mathcal{F}_1 \subseteq \mathcal{F}_2$, we obviously have:

$$P[(T, H) \in \mathcal{F}_1] \leq P[(T, H) \in \mathcal{F}_2].$$

From this it follows that:

$$\begin{aligned} P_e(\mathcal{B}, \mathcal{E}) &= \sup_{\mathcal{F} \in \mathcal{E}} \{P[(T, H) \in \mathcal{F}]\} \\ &= \sup_{\mathcal{F} \in \mathcal{E}^*} \{P[(T, H) \in \mathcal{F}]\}. \end{aligned}$$

3. Convex environmental contours

It is often natural to assume that a failure region is *convex*. This means that if the structure fails at two distinct points (t_1, h_1) and (t_2, h_2), then it also fails for all states on the straight line between these points. If the contour is convex as well, this implies that the maximal failure regions are halfspaces. See Fig. 3.1 where Π is a supporting hyperplane of the convex set $\mathcal{B}$, while Π^+ is a supporting halfspace of $\mathcal{B}$. The set Π^- is the halfspace separated from Π^+ by the hyperplane Π. We say that Π^- as the halfspace *opposite* to the supporting halfspace Π^+, and observe that $\mathcal{B} \subseteq \Pi^-$.

In the remaining parts of this paper we only consider contour sets $\mathcal{B}$ which are *compact* and *convex*. Furthermore, we assume that all the sets in $\mathcal{E}$ are *convex*. For a given compact and convex set $\mathcal{B}$ we introduce the following families of sets:

$\mathcal{P}(\mathcal{B})$ = The family of supporting hyperplanes of $\mathcal{B}$,

$\mathcal{P}^+(\mathcal{B})$ = The family of supporting halfspaces of $\mathcal{B}$,

[1] A set is *compact* if it is closed and bounded.

[2] Although this condition includes the possibility that $\mathcal{F} \cap \mathcal{B} = \partial\mathcal{B}$, the failure regions considered in the present paper will typically overlap only with a proper subset of $\partial\mathcal{B}$.

[3] The target probability is usually determined based on the relevant data sampling rate and the desired return period of a failure event. See Huseby et al. (2013) for further details. A target probability is typically a small number, e.g., of magnitude 10^{-4} or 10^{-5}. In order to avoid degenerate cases, the target probability must at least be smaller 0.5.

$\mathcal{P}^-(\mathcal{B})$ = The family of halfspaces opposite to supporting halfspaces of $\mathcal{B}$

By using well-known results from convexity theory, it is easy to show the following result:

Proposition 3.1. *Let $\mathcal{B} \subset \mathbb{R}^2$ be a compact and convex set, and let $\mathcal{E}$ be the family of convex sets such that $\mathcal{F} \cap \mathcal{B} \subseteq \partial\mathcal{B}$ for all $\mathcal{F} \in \mathcal{E}$. Then $\mathcal{E}^* = \mathcal{P}^+(\mathcal{B})$, and hence:*

$$P_e(\mathcal{B}, \mathcal{E}) = \sup_{\Pi^+ \in \mathcal{P}^+(\mathcal{B})} \{P[(T, H) \in \Pi^+]\}. \tag{3.1}$$

Moreover, the set $\mathcal{B}$ can be expressed as:

$$\mathcal{B} = \bigcap_{\Pi^- \in \mathcal{P}^-(\mathcal{B})} \Pi^-. \tag{3.2}$$

The families $\mathcal{P}(\mathcal{B})$, $\mathcal{P}^+(\mathcal{B})$ and $\mathcal{P}^-(\mathcal{B})$ can be expressed in a more explicit form. In order to explain how this can be done, we start out by letting $\theta \in [0, 2\pi)$, and define:

$$B(\mathcal{B}, \theta) = \sup_{(t,h) \in \mathcal{B}} [t\cos(\theta) + h\sin(\theta)] \tag{3.3}$$

We also introduce :

$$\Pi(\mathcal{B}, \theta) = \{(t, h) : t\cos(\theta) + h\sin(\theta) = B(\mathcal{B}, \theta)\}$$
$$\Pi^+(\mathcal{B}, \theta) = \{(t, h) : t\cos(\theta) + h\sin(\theta) \geq B(\mathcal{B}, \theta)\},$$
$$\Pi^-(\mathcal{B}, \theta) = \{(t, h) : t\cos(\theta) + h\sin(\theta) \leq B(\mathcal{B}, \theta)\}.$$

Since $\mathcal{B}$ is assumed to be compact, it follows that $\mathcal{B}$ is bounded, and thus, $B(\mathcal{B}, \theta)$ must be finite. Moreover, by the definition of $B(\mathcal{B}, \theta)$ it follows that:

$$t\cos(\theta) + h\sin(\theta) \leq B(\mathcal{B}, \theta), \quad \text{for all } (t, h) \in \mathcal{B}.$$

Finally, since $\mathcal{B}$ is compact, $\mathcal{B}$ is closed as well. Thus, there must exist at least one point $(t_0, h_0) \in \mathcal{B}$ such that:

$$t_0\cos(\theta) + h_0\sin(\theta) = B(\mathcal{B}, \theta)$$

From this it follows that $\Pi(\mathcal{B}, \theta) \in \mathcal{P}(\mathcal{B})$, $\Pi^+(\mathcal{B}, \theta) \in \mathcal{P}^+(\mathcal{B})$ and $\Pi^-(\mathcal{B}, \theta) \in \mathcal{P}^-(\mathcal{B})$.

Assume conversely that $\Pi \in \mathcal{P}(\mathcal{B})$, and let Π^+ and Π^- be the corresponding supporting and opposite halfspaces separated by Π. Then Π, Π^+ and Π^- can be expressed as follows:

$$\Pi = \{(t, h) : ta_1 + ha_2 = b\},$$
$$\Pi^+ = \{(t, h) : ta_1 + ha_2 \geq b\},$$
$$\Pi^- = \{(t, h) : ta_1 + ha_2 \leq b\}$$

for suitable real numbers a_1, a_2 and b. Without loss of generality we may assume that a_1 and a_2 are *normalized* such that $a_1^2 + a_2^2 = 1$. Then it follows that there exists a $\theta \in [0, 2\pi)$ such that $a_1 = \cos(\theta)$ and $a_2 = \sin(\theta)$.

Since Π^+ is a supporting halfspace of $\mathcal{B}$, we must have:

$$t\cos(\theta) + h\sin(\theta) \leq b, \quad \text{for all } (t, h) \in \mathcal{B},$$

and

$$t_0\cos(\theta) + h_0\sin(\theta) = b, \quad \text{for some } (t_0, h_0) \in \mathcal{B},$$

From this it follows that:

$$b = \sup_{(t,h) \in \mathcal{B}} [t\cos(\theta) + h\sin(\theta)] = B(\mathcal{B}, \theta),$$

implying that $\Pi = \Pi(\mathcal{B}, \theta)$, $\Pi^+ = \Pi^+(\mathcal{B}, \theta)$ and $\Pi^- = \Pi^-(\mathcal{B}, \theta)$. The following proposition summarizes these findings:

Proposition 3.2. *Let $\mathcal{B} \subset \mathbb{R}^2$ be a compact and convex set. Then we have:*

$$\mathcal{P}(\mathcal{B}) = \{\Pi(\mathcal{B}, \theta) : \theta \in [0, 2\pi)\},$$
$$\mathcal{P}^+(\mathcal{B}) = \{\Pi^+(\mathcal{B}, \theta) : \theta \in [0, 2\pi)\},$$
$$\mathcal{P}^-(\mathcal{B}) = \{\Pi^-(\mathcal{B}, \theta) : \theta \in [0, 2\pi)\}.$$

Furthermore, by combining Propositions 3.1 and 3.2 we also obtain the following result:

Proposition 3.3. *Let $\mathcal{B} \subset \mathbb{R}^2$ be a compact and convex set, and let $\mathcal{E}$ be the family of convex sets such that $\mathcal{F} \cap \mathcal{B} \subseteq \partial\mathcal{B}$ for all $\mathcal{F} \in \mathcal{E}$. Then we have:*

$$P_e(\mathcal{B}, \mathcal{E}) = \sup_{\theta \in [0,2\pi)} \{P[(T, H) \in \Pi^+(\mathcal{B}, \theta)]\}. \tag{3.4}$$

Moreover, the set $\mathcal{B}$ can be expressed as:

$$\mathcal{B} = \bigcap_{\theta \in [0,2\pi)} \Pi^-(\mathcal{B}, \theta) \tag{3.5}$$

An immediate consequence of this result is that the function B induces an *ordering* of compact and convex sets. More formally, we have the following result:

Proposition 3.4. *Let $\mathcal{B}_1$ and $\mathcal{B}_2$ be two compact and convex sets, and assume that:*

$B(\mathcal{B}_1, \theta) \leq B(\mathcal{B}_2, \theta)$ *for all* $\theta \in [0, 2\pi)$.

Then $\mathcal{B}_1 \subseteq \mathcal{B}_2$.

Proof. If $B(\mathcal{B}_1, \theta) \leq B(\mathcal{B}_2, \theta)$ for all $\theta \in [0, 2\pi)$, this implies that:

$\Pi^-(\mathcal{B}_1, \theta) \subseteq \Pi^-(\mathcal{B}_2, \theta)$ for all $\theta \in [0, 2\pi)$.

Hence, by the second part of Proposition 3.3 we get that:

$$\mathcal{B}_1 = \bigcap_{\theta \in [0,2\pi)} \Pi^-(\mathcal{B}_1, \theta) \subseteq \bigcap_{\theta \in [0,2\pi)} \Pi^-(\mathcal{B}_2, \theta) = \mathcal{B}_2 \quad \blacksquare$$

Another consequence of Proposition 3.3 is that a compact and convex set $\mathcal{B} \subset \mathbb{R}^2$ is uniquely determined by the function $B(\mathcal{B}, \theta)$. Hence, the boundary $\partial\mathcal{B}$ can be reconstructed from this function as well. In order to study the relation between $B(\mathcal{B}, \theta)$ and $\partial\mathcal{B}$ further, the following result, first proved by Minkowski in 1896, is relevant:

Proposition 3.5 (*Minkowski*)**.** *Let $\mathcal{B}$ be a closed convex set. Then for every point $\mathbf{x} \in \partial\mathcal{B}$ there exists a hyperplane $\Pi \in \mathcal{P}(\mathcal{B})$ such that $\mathbf{x} \in \Pi$.*

By using Proposition 3.2 this result can be restated for compact convex sets in $\mathbb{R}^2$ as follows:

Proposition 3.6. *Let $\mathcal{B} \subset \mathbb{R}^2$ be a compact convex set. Then for every point $(t_0, h_0) \in \partial\mathcal{B}$ there exists a $\theta \in [0, 2\pi)$ such that $(t_0, h_0) \in \Pi(\mathcal{B}, \theta)$.*

This proposition indicates that it may be possible to construct a mapping from angles $\theta \in [0, 2\pi)$ to the points in $\partial\mathcal{B}$. In the general case, however, the relation between angles and boundary points is not straightforward. By the definition of $B(\mathcal{B}, \theta)$ it follows that for a given $\theta \in [0, 2\pi)$ there exists at least one point $(t_0, h_0) \in \mathcal{B}$ such that:

$$t_0\cos(\theta) + h_0\sin(\theta) = B(\mathcal{B}, \theta), \tag{3.6}$$

and this point must also be on the boundary of $\mathcal{B}$. However, (t_0, h_0) may not be the only boundary point which satisfies (3.6). As an example consider a case where $\mathcal{B}$ is a convex polygon. If, for a given θ, the vector $(\cos(\theta), \sin(\theta))$ is orthogonal to, and pointing away from one of sides of $\mathcal{B}$, then the hyperplane $\Pi(\mathcal{B}, \theta)$ intersects with all the points on this side. On the other hand, for any $\theta' \neq \theta$, the corresponding supporting hyperplane $\Pi(\mathcal{B}, \theta')$ does not intersect with any of the points on this side (except possibly the endpoints). Hence, it is not possible to define a mapping where each angle $\theta \in [0, 2\pi)$ is mapped to a unique point $(t_0, h_0) \in \partial\mathcal{B}$.

In order to avoid such problems we assume that $\mathcal{B}$ is *strictly* convex. That is, for any pair of distinct points $(t_1, h_1), (t_2, h_2) \in \mathcal{B}$, all the points on the line segment between (t_1, h_1) and (t_2, h_2) (except possibly the endpoints (t_1, h_1) and (t_2, h_2)) belong to the interior of $\mathcal{B}$. The following proposition essentially states that for strictly convex sets there exists a well-defined mapping from angles to boundary points.

Proposition 3.7. *Let $\mathcal{B} \subset \mathbb{R}^2$ be a compact and strictly convex set. Then for every angle $\theta \in [0, 2\pi)$ there exists a unique point $(t(\theta), h(\theta)) \in \partial\mathcal{B}$ such that $(t(\theta), h(\theta)) \in \Pi(\mathcal{B}, \theta)$.*

Proof. By the definition of $\Pi(\mathcal{B}, \theta)$ we know that there exists at least one point $(t_1, h_1) \in \partial\mathcal{B}$ such that $(t_1, h_1) \in \Pi(\mathcal{B}, \theta)$. Assume, for a contradiction that there exists another boundary point (t_2, h_2), different from (t_1, h_1), which also belongs to the hyperplane $\Pi(\mathcal{B}, \theta)$. Since $\Pi(\mathcal{B}, \theta)$ is convex, all the points on the line segment between (t_1, h_1) and (t_2, h_2) also belong to $\Pi(\mathcal{B}, \theta)$. However, since $\mathcal{B}$ is assumed to be strictly convex, the points on the line segment between (t_1, h_1) and (t_2, h_2) are elements of the interior of $\mathcal{B}$, which contradicts that $\Pi(\mathcal{B}, \theta)$ is a supporting hyperplane of $\mathcal{B}$. Hence, we conclude that $(t_1, h_1) \in \partial\mathcal{B}$ is the only boundary point which intersects with $\Pi(\mathcal{B}, \theta)$, and we define $(t(\theta), h(\theta))$ to be this point ■

If the function $B(\mathcal{B}, \cdot)$ is differentiable, the mapping from angles to boundary points is given by the following explicit formula:

Proposition 3.8. *Let $\mathcal{B} \subset \mathbb{R}^2$ be a compact and strictly convex set, and assume that $B(\mathcal{B}, \cdot)$ defined by (3.3) is differentiable. Then the boundary of $\mathcal{B}$ can be expressed as:*

$$\partial\mathcal{B} = \{(t(\theta), h(\theta)) : \theta \in [0, 2\pi)\}$$

where:

$$\begin{pmatrix} t(\theta) \\ h(\theta) \end{pmatrix} = \begin{bmatrix} B(\mathcal{B}, \theta) & -B'(\mathcal{B}, \theta) \\ B'(\mathcal{B}, \theta) & B(\mathcal{B}, \theta) \end{bmatrix} \cdot \begin{pmatrix} \cos(\theta) \\ \sin(\theta) \end{pmatrix}. \tag{3.7}$$

Proof. See Huseby et al. (2015a) ■

The function $B(\mathcal{B}, \cdot)$ introduced in (3.3) can be extended to a function defined for all $\theta \in \mathbb{R}$. Since the trigonometric functions $\cos(\cdot)$ and $\sin(\cdot)$ are periodic, the extended version of $B(\mathcal{B}, \cdot)$ is periodic as well and have the property that $B(\mathcal{B}, \theta) = B(\mathcal{B}, \theta \pm 2\nu\pi)$ for all $\nu \in \mathbb{N}$. Since the set $\mathcal{B}$ is convex, the function $B(\mathcal{B}, \cdot)$ must satisfy a certain condition. In order to investigate this further we assume that the $B(\mathcal{B}, \cdot)$ is two times differentiable, and consider the derivative of $(t(\theta), h(\theta))$ with respect to θ. By (3.7) we get that:

$$\begin{aligned} t'(\theta) &= B'(\mathcal{B}, \theta)\cos(\theta) - B(\mathcal{B}, \theta)\sin(\theta) \\ &\quad - B''(\mathcal{B}, \theta)\sin(\theta) - B'(\mathcal{B}, \theta)\cos(\theta) \\ &= -[B(\mathcal{B}, \theta) + B''(\mathcal{B}, \theta)]\sin(\theta) \\ h'(\theta) &= B''(\mathcal{B}, \theta)\cos(\theta) - B'(\mathcal{B}, \theta)\sin(\theta) \\ &\quad + B'(\mathcal{B}, \theta)\sin(\theta) + B(\mathcal{B}, \theta)\cos(\theta) \\ &= [B(\mathcal{B}, \theta) + B''(\mathcal{B}, \theta)]\cos(\theta). \end{aligned}$$

That is, we have:

$$\begin{pmatrix} t'(\theta) \\ h'(\theta) \end{pmatrix} = [B(\mathcal{B}, \theta) + B''(\mathcal{B}, \theta)] \cdot \begin{pmatrix} -\sin(\theta) \\ \cos(\theta) \end{pmatrix}. \tag{3.8}$$

In order to prove the convexity condition for $B(\mathcal{B}, \cdot)$, we need the following lemmas:

Lemma 3.9. *Let $\mathcal{B} \subset \mathbb{R}^2$ be a compact and strictly convex set, and let:*

$$\tilde{\mathcal{B}} = \{(\tilde{t}, \tilde{h}) = (t - t_0, h - h_0) : (t, h) \in \mathcal{B}\} \tag{3.9}$$

for some point $(t_0, h_0) \in \mathbb{R}^2$. Then $B(\tilde{\mathcal{B}}, \theta)$ is given by:

$$B(\tilde{\mathcal{B}}, \theta) = B(\mathcal{B}, \theta) - t_0\cos(\theta) - h_0\sin(\theta),$$

for all $\theta \in \mathbb{R}$. Moreover, assuming that $B(\mathcal{B}, \cdot)$ is two times differentiable, we have:

$$\begin{aligned} B'(\tilde{\mathcal{B}}, \theta) &= B'(\mathcal{B}, \theta) + t_0\sin(\theta) - h_0\cos(\theta), \\ B''(\tilde{\mathcal{B}}, \theta) &= B''(\mathcal{B}, \theta) + t_0\cos(\theta) + h_0\sin(\theta). \end{aligned}$$

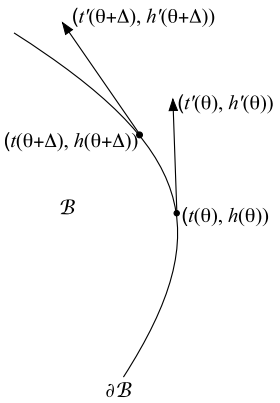

Fig. 3.2. Derivatives.

Proof. By (3.3) we have:

$$\begin{aligned} B(\tilde{\mathcal{B}}, \theta) &= \sup_{(\tilde{t}, \tilde{h}) \in \tilde{\mathcal{B}}} \{\tilde{t}\cos(\theta) + \tilde{h}\sin(\theta)\} \\ &= \sup_{(t, h) \in \mathcal{B}} \{(t - t_0)\cos(\theta) + (h - h_0)\sin(\theta)\} \\ &= \sup_{(t, h) \in \mathcal{B}} \{t\cos(\theta) + h\sin(\theta)\} - t_0\cos(\theta) - h_0\sin(\theta) \\ &= B(\mathcal{B}, \theta) - t_0\cos(\theta) - h_0\sin(\theta) \end{aligned}$$

The remaining parts of the lemma follow by taking derivatives ■

Lemma 3.10. *Let $\mathcal{B} \subset \mathbb{R}^2$ be a compact and strictly convex set, and assume that $B(\mathcal{B}, \cdot)$ is two times differentiable. Then there exists a $\theta_0 \in (0, 2\pi)$ such that:*

$$B(\mathcal{B}, \theta_0) + B''(\mathcal{B}, \theta_0) > 0.$$

Proof. Let (t_0, h_0) be an interior point of $\mathcal{B}$ and let $\tilde{\mathcal{B}}$ be defined as in (3.9). Then we have:

$$t_0\cos(\theta) + h_0\sin(\theta) < B(\mathcal{B}, \theta) \quad \text{for all } \theta \in [0, 2\pi)$$

Hence, by Lemma 3.9 we have:

$$B(\tilde{\mathcal{B}}, \theta) = B(\mathcal{B}, \theta) - t_0\cos(\theta) - h_0\sin(\theta) > 0 \quad \text{for all } \theta \in [0, 2\pi)$$

Moreover, since $B(\tilde{\mathcal{B}}, \theta)$ extended to a function defined for all $\theta \in \mathbb{R}$, is periodic, it follows that the extended version of $B'(\tilde{\mathcal{B}}, \theta)$ is periodic as well. In particular that $B'(\tilde{\mathcal{B}}, 0) = B'(\tilde{\mathcal{B}}, 2\pi)$. Hence, by the mean value theorem, there exists a $\theta_0 \in (0, 2\pi)$ such that $B''(\tilde{\mathcal{B}}, \theta_0) = 0$. From this it follows that:

$$B(\tilde{\mathcal{B}}, \theta_0) + B''(\tilde{\mathcal{B}}, \theta_0) > 0$$

By Lemma 3.9 we also that:

$$\begin{aligned} B(\tilde{\mathcal{B}}, \theta_0) + B''(\tilde{\mathcal{B}}, \theta_0) &= B(\mathcal{B}, \theta_0) - t_0\cos(\theta) - h_0\sin(\theta) \\ &\quad + B''(\mathcal{B}, \theta_0) + t_0\cos(\theta) + h_0\sin(\theta) \\ &= B(\mathcal{B}, \theta_0) + B''(\mathcal{B}, \theta_0), \end{aligned}$$

and thus, the result follows ■

As θ runs through $[0, 2\pi)$, the point $(t(\theta), h(\theta))$ runs counterclockwise through the boundary $\partial\mathcal{B}$. The derivative $(t'(\theta), h'(\theta))$ is the tangent vector to $\partial\mathcal{B}$ at $(t(\theta), h(\theta))$.

Since the set $\mathcal{B}$ is assumed to be strictly convex, the angle between $(t'(\theta), h'(\theta))$ and $(t'(\theta + \Delta), h'(\theta + \Delta))$ is positive for any $\theta \in [0, 2\pi)$ and small $\Delta > 0$ (see Fig. 3.2). We then define:

$$\boldsymbol{\nu}(\theta) = (t'(\theta), h'(\theta), 0), \quad \theta \in [0, 2\pi),$$

and calculate the cross-product:

$$\boldsymbol{v}(\theta)\times\boldsymbol{v}(\theta+\Delta)=\begin{vmatrix} \boldsymbol{i} & \boldsymbol{j} & \boldsymbol{k} \\ t'(\theta) & h'(\theta) & 0 \\ t'(\theta+\Delta) & h'(\theta+\Delta) & 0 \end{vmatrix}$$
$$=(0,\,0,\,t'(\theta)\cdot h'(\theta+\Delta)-h'(\theta)\cdot t'(\theta+\Delta))$$

By the *right-hand rule* of the cross-product the angle between the vectors $(t'(\theta),h'(\theta),0)$ and $(t'(\theta+\Delta),h'(\theta+\Delta),0)$ is positive if and only if:

$$t'(\theta)\cdot h'(\theta+\Delta)-h'(\theta)\cdot t'(\theta+\Delta)>0.$$

Inserting the expressions for the derivatives given in (3.8) we get:

$$\begin{aligned} &t'(\theta)\cdot h'(\theta+\Delta)-h'(\theta)\cdot t'(\theta+\Delta)\\ &\quad=[B(\mathcal{B},\theta)+B''(\mathcal{B},\theta)]\cdot[B(\mathcal{B},\theta+\Delta)+B''(\mathcal{B},\theta+\Delta)]\\ &\qquad\cdot(-\sin(\theta)\cos(\theta+\Delta)+\sin(\theta+\Delta)\cos(\theta))\\ &\quad=[B(\mathcal{B},\theta)+B''(\mathcal{B},\theta)]\cdot[B(\mathcal{B},\theta+\Delta)+B''(\mathcal{B},\theta+\Delta)]\cdot\sin(\Delta). \end{aligned}$$

Since $\Delta>0$ is small, we have $\sin(\Delta)>0$. Hence, the angle between $(t'(\theta),h'(\theta))$ and $(t'(\theta+\Delta),h'(\theta+\Delta))$ is positive if and only if:

$$[B(\mathcal{B},\theta)+B''(\mathcal{B},\theta)]\cdot[B(\mathcal{B},\theta+\Delta)+B''(\mathcal{B},\theta+\Delta)]>0$$

for all $\theta\in[0,2\pi)$ and small $\Delta>0$. This condition holds if and only if the sign of $B(\mathcal{B},\theta)+B''(\mathcal{B},\theta)$ is the same for all $\theta\in[0,2\pi)$.

By Lemma 3.10 there exists at least one $\theta_0\in(0,2\pi)$ such that $B(\mathcal{B},\theta_0)+B''(\mathcal{B},\theta_0)>0$. Hence, we have shown the following important result:

Theorem 3.11. *Let $\mathcal{B}\subset\mathbb{R}^2$ be a compact and strictly convex set, and assume that $B(\mathcal{B},\cdot)$ is two times differentiable. Then we have:*

$$B(\mathcal{B},\theta)+B''(\mathcal{B},\theta)>0 \text{ for all } \theta\in[0,2\pi). \tag{3.10}$$

Given a periodic function which does not satisfy (3.10), it is very easy to modify this function so that the condition is satisfied. The following result shows how this can be done.

Proposition 3.12. *Let $C(\cdot)$ be a periodic function with period 2π which is two times differentiable. Assuming that both C and C'' are bounded, there exists a constant C_0 such that the function $\tilde{C}(\cdot)=C_0+C(\cdot)$ satisfies (3.10).*

Proof. We let:

$$c=\inf_{\theta\in[0,2\pi)}[C(\theta)+C''(\theta)]$$

Since both C and C'' are bounded, c must be finite. If $c>0$, $C(\cdot)$ satisfies (3.10). We may then let $C_0=0$. Hence, $\tilde{C}(\cdot)=C(\cdot)$, and thus, $\tilde{C}(\cdot)$ obviously satisfies (3.10) as well. On the other hand, if $c\le 0$, we let C_0 be some number greater than $-c$. Since $\tilde{C}''=C''$, it follows that for all $\theta\in[0,2\pi)$ we have:

$$\begin{aligned} \tilde{C}(\theta)+\tilde{C}''(\theta)&=C_0+C(\theta)+C''(\theta)\\ &>-c+C(\theta)+C''(\theta)\\ &\ge -c+c=0. \end{aligned}$$

Hence, we conclude that $\tilde{C}(\cdot)$ satisfies (3.10) ■

3.1. Valid convex environmental contours

We now turn to the problem of finding a convex contour $\partial\mathcal{B}$ which is *valid*, i.e., a contour that has an exceedance probability which is less than or equal to a given target probability $p_e\in(0,0.5)$.

Following Huseby et al. (2015a) we let $C(\theta)$ be defined for all angles $\theta\in[0,2\pi)$ as:

$$C(\theta)=\inf\{y:\,P[Y(\theta)>y]\le p_e\}, \tag{3.11}$$

where $Y(\theta)=T\cos(\theta)+H\sin(\theta)$. The function C is referred to as the p_e-level *percentile function* of the joint distribution of (T,H).

For $\theta\in[0,2\pi)$ we also introduce :

$$\begin{aligned} \Pi(\theta)&=\{(t,h):\,t\cos(\theta)+h\sin(\theta)=C(\theta)\}\\ \Pi^+(\theta)&=\{(t,h):\,t\cos(\theta)+h\sin(\theta)\ge C(\theta)\},\\ \Pi^-(\theta)&=\{(t,h):\,t\cos(\theta)+h\sin(\theta)\le C(\theta)\}. \end{aligned}$$

By the definition of $C(\theta)$ and the assumption that the distribution of (T,H) is absolutely continuous with respect to the Lebesgues measure in $\mathbb{R}^2$ it follows that for all $\theta\in[0,2\pi)$ we have:

$$\begin{aligned} &P[(T,H)\in\Pi^+(\theta)]\\ &\quad=P[T\cos(\theta)+H\sin(\theta)\ge C(\theta)]\\ &\quad=P[T\cos(\theta)+H\sin(\theta)>C(\theta)]=p_e \end{aligned}$$

If we can find a convex set $\mathcal{B}$ such that $B(\mathcal{B},\theta)\ge C(\theta)$, it follows by Proposition 3.3 that:

$$\begin{aligned} P_e(\mathcal{B},\mathcal{E})&=\sup_{\theta\in[0,2\pi)}\{P[(T,H)\in\Pi^+(\mathcal{B},\theta)]\}\\ &=\sup_{\theta\in[0,2\pi)}\{P[T\cos(\theta)+H\sin(\theta)\ge B(\mathcal{B},\theta)]\}\\ &\le\sup_{\theta\in[0,2\pi)}\{P[T\cos(\theta)+H\sin(\theta)\ge C(\theta)]\}=p_e \end{aligned}$$

Hence, this implies that $\partial\mathcal{B}$ is a valid environmental contour. As stated Section 2 our goal is to find a *minimal* set $\mathcal{B}$ such that $\partial\mathcal{B}$ is valid. By Proposition 3.4 this means that we want $B(\mathcal{B},\theta)$ to be as small as possible. Thus, if there exists a compact and convex set $\mathcal{B}$ such that $B(\mathcal{B},\theta)=C(\theta)$ for all $\theta\in[0,2\pi)$, this set will be the minimal compact and convex set with the property that $\partial\mathcal{B}$ is a valid environmental contour. The following result summarizes the consequences of all these findings:

Theorem 3.13. *Let $C(\cdot)$ be defined by (3.11), and assume that there exists a compact and convex set $\mathcal{B}$ such that $B(\mathcal{B},\theta)=C(\theta)$ for all $\theta\in[0,2\pi)$. Then $\mathcal{B}$ is the minimal compact and convex set with the property that $\partial\mathcal{B}$ is a valid environmental contour, and the set $\mathcal{B}$ is given by:*

$$\mathcal{B}=\bigcap_{\theta\in[0,2\pi)}\Pi^-(\theta) \tag{3.12}$$

If $\mathcal{B}$ is strictly convex, and $C(\cdot)$ is differentiable, the environmental contour, $\partial\mathcal{B}$, can be expressed as:

$$\partial\mathcal{B}=\{(t(\theta),h(\theta)):\,\theta\in[0,2\pi)\},$$

where:

$$\begin{pmatrix} t(\theta)\\ h(\theta)\end{pmatrix}=\begin{bmatrix} C(\theta) & -C'(\theta)\\ C'(\theta) & C(\theta)\end{bmatrix}\cdot\begin{pmatrix}\cos(\theta)\\ \sin(\theta)\end{pmatrix}, \tag{3.13}$$

If $C(\cdot)$ is two times differentiable, a necessary condition for the existence of a strictly convex set $\mathcal{B}$ such that $B(\mathcal{B},\theta)=C(\theta)$ for all $\theta\in[0,2\pi)$ is that:

$$C(\theta)+C''(\theta)>0 \text{ for all } \theta\in[0,2\pi). \tag{3.14}$$

Note that the function $C(\cdot)$ is determined by the joint distribution of T and H. It is possible to construct distributions where $C(\cdot)$ does not satisfy (3.14). In such cases the contour defined by the formula (3.13), will not be the boundary of a convex set. When this happens, $C(\cdot)$ must be adjusted. We will return to this issue in Section 5.

In this section we have studied environmental contours defined through the p_e-level percentile function (3.11). Theorem 3.13 shows that if a minimal valid environmental contour exists (for some given joint distribution of (T,H)), then it is necessarily given by the representation (3.13), and that the differential inequality (3.14) has to hold. In Section 5 we will see that the condition (3.14) is useful for analysing and improving numerical methods for constructing environmental contours. This is also true in higher dimensions, i.e. when instead of $(T,H)\in\mathbb{R}^2$ one considers a random variable in $\mathbb{R}^m$. By studying the connection between environmental contours and Voronoi cells, Hafver et al. (2020) proved the n-dimensional analog of (3.13) and a slightly weaker alternative of the necessary condition (3.14) (corresponding to $\ge$ in (3.14)). This method is also discussed further in Sections 4 and 5.

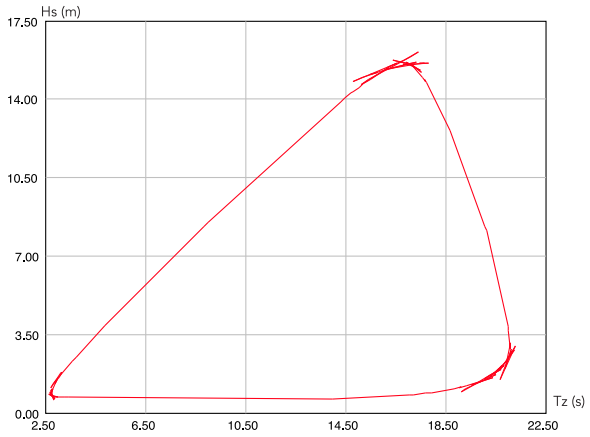

Fig. 4.1. $N = 1000$ simulations, $n = 90$ angles.

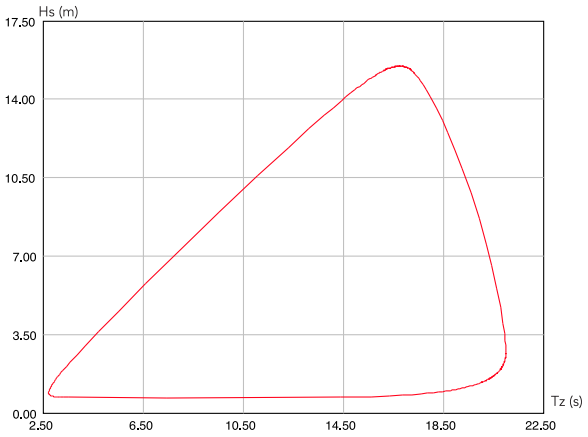

Fig. 4.2. $N = 1000000$ simulations, $n = 360$ angles.

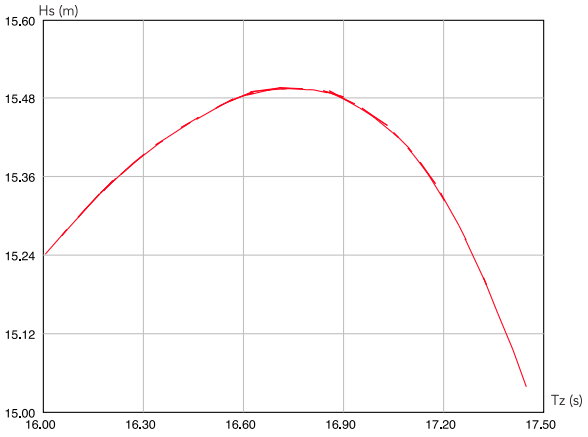

Fig. 4.3. $N = 1000000$ simulations, $n = 360$ angles.

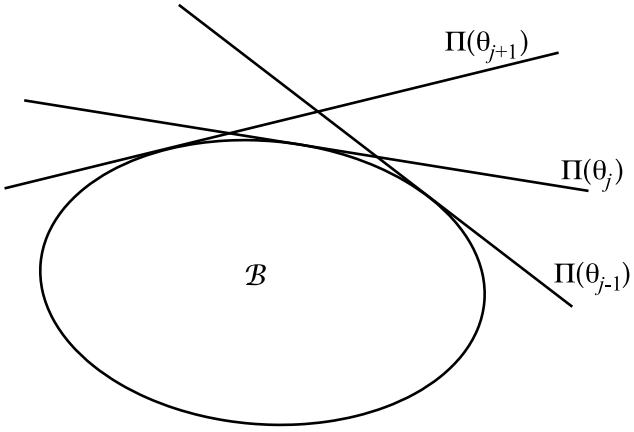

Fig. 4.4. Ideal case: All hyperplanes support $\mathcal{B}$.

4. Estimating environmental contours

In a given practical situation the C-function is typically estimated pointwise using Monte Carlo simulations. Following Huseby et al. (2015a) we assume that we have a sample from the joint distribution of (T, H) generated using Monte Carlo simulation:

$$(T_1, H_1), \dots, (T_N, H_N)$$

For a given angle $\theta \in [0, 2\pi)$ we calculate the projections of these points onto the unit vector $(\cos(\theta), \sin(\theta))$, i.e.:

$$Y_j(\theta) = T_j \cos(\theta) + H_j \sin(\theta), \quad j = 1, \dots, N$$

These projections are then sorted in ascending order:

$$Y_{(1)}(\theta) \le Y_{(2)}(\theta) \le \cdots \le Y_{(N)}(\theta).$$

Assuming that $k \le N$ is an integer such that:

$$\frac{k}{N} \approx 1 - p_e,$$

it follows that $C(\theta)$ can be estimated by:

$$\hat{C}(\theta) = Y_{(k)}(\theta) \tag{4.1}$$

Proceeding in this fashion the C-function can be estimated for a suitable set of angles $\theta_1, \dots, \theta_n \in [0, \pi)$. We let $\hat{C}(\theta_1), \dots, \hat{C}(\theta_n)$ denote the resulting estimates. The set $\mathcal{B}$ given in (3.12) of Theorem 3.13 can then be approximated by a polygon of the following form:

$$\hat{\mathcal{B}} = \bigcap_{i=1}^{n} \hat{H}^-(\theta_i), \tag{4.2}$$

where:

$$\hat{H}^-(\theta_i) = \{(t, h) : t \cos(\theta) + h \sin(\theta) \le \hat{C}(\theta_i)\}$$

There are several methods for constructing an estimate of the boundary of the set $\mathcal{B}$. One method is based directly on the polygon given in (4.2), where the corners are determined by computing the intersection between the hyperplanes $\Pi(\theta_i)$ and $\Pi(\theta_{i+1})$, for $i = 1, \dots, n$, and where we define $\Pi(\theta_{n+1})$ to be equal to $\Pi(\theta_1)$. This method is also similar to the method suggested by Ottesen and Aarstein (2006), and is the method used in the remaining part of the present paper. Another method is based on (3.13) given in Theorem 3.13. This method uses the estimate of the p_e-level percentile function given in (4.1). Other methods include the use of Fourier series and splines. For more details on this see Huseby et al. (2015a).

In Fig. 4.1 the set $\mathcal{B}$ is estimated using only a few simulations and halfspaces. We observe that the resulting contour has significant irregularities especially in the areas where the direction of the contour changes a lot.

By increasing the number of simulations and halfspaces, a smoother contour is obtained. This is illustrated in Fig. 4.2. If we zoom in on the border of $\hat{\mathcal{B}}$, we still find substantial "irregularities" as is seen in Fig. 4.3. This issue is illustrated in a simplified way in Fig. 4.4 and Fig. 4.5. Fig. 4.4 represents an ideal case where all the hyperplanes support $\mathcal{B}$. In such cases $\mathcal{B}$ is well approximated by the polygon obtained as the intersection of the corresponding halfspaces. The corners of the polygon are obtained as the intersection points between successive hyperplanes, and the boundary of the polygon is obtained by drawing

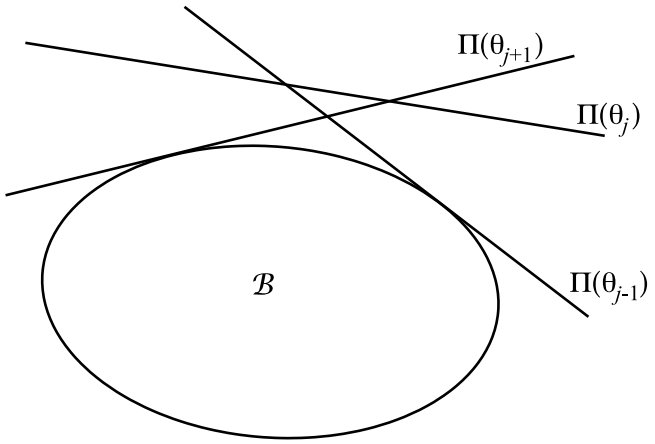

Fig. 4.5. Irregular case: The hyperplane $\Pi(\theta_j)$ does *not* support $\mathcal{B}$.

straight lines between the corners. Since all the hyperplanes support $\mathcal{B}$, no loops occur. Fig. 4.5 on the other hand represents a case where at least one of the hyperplanes does not support $\mathcal{B}$. Attempting to obtain the boundary of the polygon by drawing straight lines between the intersection points will result in a loop. Moreover, if we use the intersection of the halfspaces as our set $\mathcal{B}$, this set will typically have a slightly higher exceedance probability than the desired value p_e. In Section 5 we will show how to avoid these problems and obtain a smooth contour.

4.1. Importance sampling, omission factors and mixtures

Generating a sample from the joint distribution of (T, H) can of course be done easily using standard Monte Carlo methods. In the following we focus on one specific method for doing this based on the Rosenblatt transformation introduced in Rosenblatt (1952). This transformation, which we here denote by Ψ, has the property that if $(X, Y) = \Psi(T, H)$, then (X, Y) is a vector of two independent standard normally distributed variables. This implies that we can generate a sample $(T_1, H_1), \dots, (T_N, H_N)$ by generating a sample of N vectors of independent standard normally distributed variables, $(X_1, Y_1), \dots, (X_N, Y_N)$, and then let $(T_j, H_j) = \Psi^{-1}(X_j, Y_j)$, $j = 1, \dots, N$. More specifically, the inverse Rosenblatt transformation, Ψ^{-1} takes the following form for $j = 1, \dots, N$:

$$H_j = F_H^{-1}(\Phi(X_j)),$$
$$T_j = F_{T|H}^{-1}(\Phi(Y_j)),$$

where Φ denotes the cumulative distribution function of the standard normal distribution, while F_H^{-1} and $F_{T|H}^{-1}$ are respectively the inverse cumulative distribution function of H and the inverse conditional cumulative distribution function of T.

We then recall that the C-function corresponds to the $(1 - p_e)$-percentiles of the projections $Y_1(\theta), \dots, Y_N(\theta)$. Thus, in order to estimate this function, only the tail area of the joint distribution of (T, H) is of interest. Huseby et al. (2015b) proposed a method for sampling from the tail based on *rejection*. We now show how this method can be improved significantly by using *importance sampling*. The idea is to generate the sample $(X_1, Y_1), \dots, (X_N, Y_N)$ from the distribution of (X, Y) conditioned on the event that the length of the vector, $\sqrt{X^2 + Y^2}$ is greater than some suitable number r, i.e., the event that the point (X, Y) falls outside of a circle $\mathcal{O}$ centred at the origin and with radius r. In order to generate $(X_1, Y_1), \dots, (X_N, Y_N)$ from this conditional distribution we use a modified Box–Muller transform. That is, we start out by generating a set of N independent vectors $(U_1, V_1), \dots, (U_N, V_N)$ where U_j and V_j are independent and uniformly distributed on the interval $(0, 1]$, $j = 1, \dots, N$. Then the desired variables are obtained by using the following transformation for $j = 1, \dots, N$:

$$X_j = \sqrt{r^2 - 2\ln(U_j)} \cdot \cos(2\pi V_j),$$
$$Y_j = \sqrt{r^2 - 2\ln(U_j)} \cdot \sin(2\pi V_j).$$

Having generated $(X_1, Y_1), \dots, (X_N, Y_N)$ we proceed by using the inverse Rosenblatt transformation, and obtain $(T_1, H_1), \dots, (T_N, H_N)$, as well as the projections $Y_1(\theta), \dots, Y_N(\theta)$.

We note that since $X_j^2 + Y_j^2$ is χ^2-distributed with 2 degrees of freedom, it follows that:

$$P((X_j, Y_j) \notin \mathcal{O}) = P(X_j^2 + Y_j^2 > r^2) = e^{-r^2/2}.$$

Assuming that the radius r is not too large, the event $\{Y_j(\theta) > C(\theta)\}$ is contained in the event that $\{(X_j, Y_j) \notin \mathcal{O}\}$, and thus, it follows that:

$$P(Y_j(\theta) > C(\theta) | (X_j, Y_j) \notin \mathcal{O}) = \frac{P(Y_j(\theta) > C(\theta))}{P((X_j, Y_j) \notin \mathcal{O})} = p_e e^{r^2/2}$$

Hence, we can estimate $C(\theta)$ by $Y_{(k')}(\theta)$ where k' is chosen so that:

$$\frac{k'}{N} \approx 1 - p_e e^{r^2/2}$$

To find a suitable value for the radius r, we express this quantity as:

$$r = \alpha\sqrt{-2\ln(p_e)}$$

for some suitable constant $\alpha > 0$. This implies that:

$$p_e e^{r^2/2} = p_e e^{-\alpha^2 \ln(p_e)} = p_e^{1-\alpha^2}$$

Since $p_e^{1-\alpha^2}$ is a probability, it follows that we must have $\alpha \leq 1$. Moreover, we observe that the radius r grows proportionally to α. A high value of α implies an aggressive importance sampling where a large portion of the data set is sampled from the tail area. In order to maximize the effect of the importance sampling we want α to be as close to 1 as possible. However, at the same time we must ensure that the event $\{Y_j(\theta) > C(\theta)\}$ is contained in the event that $\{(X_j, Y_j) \notin \mathcal{O}\}$. Experience has shown that $\alpha = 0.95$ is a good choice for most applications.

The use of importance sampling indeed has a *very significant* effect on the precision of the Monte Carlo method. Thus, using this method whenever possible is definitely desirable. Since the Rosenblatt transformation plays an important part in this method, we need to implement this transformation for the given joint distribution of the environmental variables. As a part of this, we need to determine the inverse cumulative distribution of (T, H). For most commonly used distributions, this is very easy. In some cases, however, it may be necessary to implement this using numerical methods. We will illustrate this by considering two examples.

The first example is motivated by the notion of *omission factors*. Such factors may be necessary in order to account for short-term uncertainty which is not covered by the significant wave height H. This can be done by letting $H' = H + \epsilon$, where ϵ is a suitable error term. The Rosenblatt transformation can then be expressed as:

$$H' = F_{H'}^{-1}(\Phi(X))$$
$$T = F_{T|H'}^{-1}(\Phi(Y))$$

Hence, to calculate H' we need to find the cumulative distribution function of the sum of H and ϵ, and then also the inverse of this function. Finding analytical expressions for these function is often not possible. Thus, a numerical solution is needed. Fortunately, this is usually fairly easy. In particular, if the distribution of the error term can be approximated by a discrete distribution, the resulting cumulative distribution function of H' can be represented as a discrete mixture of distribution functions. More specifically, assume that the error term has

values in the set $\{e_1, \dots, e_\ell\}$, and that $P(\epsilon = e_j) = \alpha_j$, $j = 1, \dots, \ell$. The cumulative distribution function of H' is then given by:

$$F_{H'}(h) = \sum_{j=1}^{\ell} \alpha_j F_H(h - e_j)$$

Below we describe a general method for determining the inverse of such mixtures.

In the second example we consider a case where the joint distribution of (T, H) is a discrete mixture of distributions. In addition to cases with omission factors, such mixtures occur in situations where the joint distribution depends on some background variable such as the season or the wind direction. An example of this can be found in Vanem and Huseby (2018). See also Winterstein (2016). In such cases it may not be possible to find explicit formulas for F_H^{-1} and $F_{T|H}^{-1}$. Instead one has to find the inverse by solving an equation numerically. Here we explain how to do this for F_H^{-1}. The corresponding procedure for $F_{T|H}^{-1}$ is completely similar. More specifically, we assume that $F_{H,1}, \dots, F_{H,\ell}$ are ℓ cumulative distribution functions which are all continuous and strictly increasing. Moreover, we assume that the inverse functions $F_{H,1}^{-1}, \dots, F_{H,\ell}^{-1}$ are known and easy to calculate. We have started out by generating a bivariate normal vector, (X, Y), where $X = x$, and we want to compute the corresponding value for H, i.e., $h = F_H^{-1}(x)$, and we introduce:

$$h_j = F_{H,j}^{-1}(x), \quad j = 1, \dots, \ell.$$

We also define:

$$h_{min} = \min_{1 \le j \le \ell} h_j, \text{ and } h_{max} = \max_{1 \le j \le \ell} h_j.$$

We then introduce the cumulative distribution function for H as the mixture of $F_{H,1}, \dots, F_{H,\ell}$:

$$F_H(h) = \sum_{j=1}^{\ell} \alpha_j F_{H,j}(h),$$

where $\alpha_j \ge 0$, $j = 1, \dots, \ell$, and $\sum_{j=1}^{\ell} \alpha_j = 1$.

In order to determine h we must to solve the following equation:

$$F_H(h) = \sum_{j=1}^{\ell} \alpha_j F_{H,j}(h) = x. \tag{4.3}$$

Under these assumptions there exists a unique solution to (4.3), and we have:

$$h_{min} \le h \le h_{max}. \tag{4.4}$$

To prove (4.4) we note that since the cumulative distribution functions are non-decreasing and $\sum_{j=1}^{\ell} \alpha_j = 1$, we have:

$$F_H(h_{min}) = \sum_{j=1}^{\ell} \alpha_j F_{H,j}(h_{min}) \le \sum_{j=1}^{\ell} \alpha_j F_{H,j}(h_j) = \sum_{j=1}^{\ell} \alpha_j x = x$$

Similarly, we have:

$$F_H(h_{max}) = \sum_{j=1}^{\ell} \alpha_j F_{H,j}(h_{max}) \ge \sum_{j=1}^{\ell} \alpha_j F_{H,j}(h_j) = \sum_{j=1}^{\ell} \alpha_j x = x$$

Since $F_{H,1}, \dots, F_{H,\ell}$ are continuous and strictly increasing, it follows that F_H is continuous and strictly increasing as well. Thus, since we have established that:

$$F_H(h_{min}) \le x \le F_H(h_{max})$$

there must exist some $h \in [h_{min}, h_{max}]$ such that $F_H(h) = x$.

Having identified the interval $[h_{min}, h_{max}]$ containing the solution to (4.3), the value h can easily and efficiently be found numerically, e.g., by using the bisection method.

Table 5.1
Fitted parameter for the three-parameter Weibull distribution.

α	β	γ
2.259	1.285	0.701

Table 5.2
Fitted parameter for the conditional log-normal distribution.

	$i = 1$	$i = 2$	$i = 3$
a_i	1.069	0.898	0.243
b_i	0.025	0.263	−0.148

5. Constructing a smooth environmental contour

In this section we will show how the loops illustrated in the previous sections can be removed. We demonstrate the method by considering a specific example. In this example we let $p_e = 1.37 \cdot 10^{-5}$, which corresponds to a return period of 25 years and a data collection rate of 8 observations per day. The contour is estimated using the importance sampling method presented in Section 4.1.

The joint long-term models for *significant wave height*, denoted by H, and *wave period* denoted by T is given by:

$$f_{T,H}(t, h) = f_H(h) f_{T|H}(t|h)$$

where a three-parameter Weibull distribution is used for the significant wave height, H, and a lognormal conditional distribution is used for the wave period, T.

The Weibull distribution is parameterized by a location parameter, γ, a scale parameter α, and a shape parameter β:

$$f_H(h) = \frac{\beta}{\alpha} \left(\frac{h - \gamma}{\alpha} \right)^{\beta - 1} e^{-[(h-\gamma)/\alpha]^\beta}, \quad h \ge \gamma.$$

The lognormal distribution has two parameters, the log-mean μ and the log-standard deviation σ and is expressed as:

$$f_{T|H}(t|h) = \frac{1}{t\sqrt{2\pi}} e^{-[(\ln(t)-\mu)^2/(2\sigma^2)]}, \quad t \ge 0,$$

The dependence between H and T is modelled by letting the parameters μ and σ be expressed in terms of H as follows:

$$\mu = E[\ln(T)|H = h] = a_1 + a_2 h^{a_3},$$

$$\sigma = SD[\ln(T)|H = h] = b_1 + b_2 e^{b_3 h}.$$

The parameters are estimated using available data from the relevant geographical location and are listed in Tables 5.1 and 5.2.

The resulting environmental contour, based on 1 million simulations, importance sampling and $n = 360$ hyperplanes, is illustrated in Fig. 5.1. While this contour may appear to be very smooth, it turns out that is not at all the case.

In order to show this we measure the angle between successive sides of the polygon. For a convex polygon, these angles should all be non-negative. In the simple polygon with just six corners shown in Fig. 5.2 we observe that all angles are positive except the angle at corner e. As a result the polygon is clearly not convex.

In Fig. 5.3 we have plotted the angles found at the 360 corners of the contour shown in Fig. 4.2. Due to a high number of loops in some areas we see that a substantial number of the angles are indeed negative.

Since the estimated environmental contours shown here are polygons, these sets are clearly not strictly convex. Still it turns out the loop issue is strongly connected to the necessary condition for strict convexity given in (3.14) in Theorem 3.13. In order to study this further we have estimated values of $C(\theta)+C''(\theta)$ using interpolation and plotted the resulting curve in Fig. 5.4. We observe that the curve values are mostly positive except for some clusters of small negative values. It is these negative values that cause the loops.

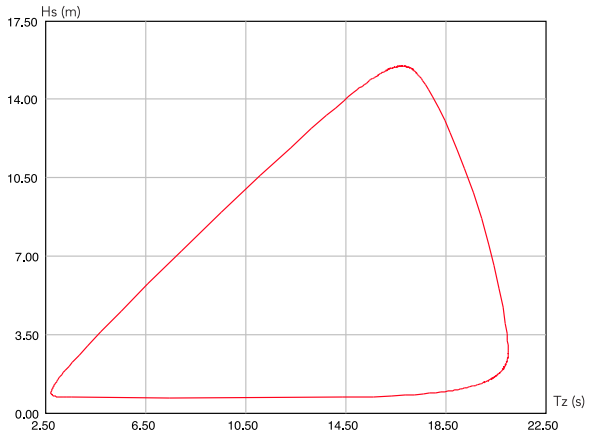

Fig. 5.1. Environmental contour before smoothing.

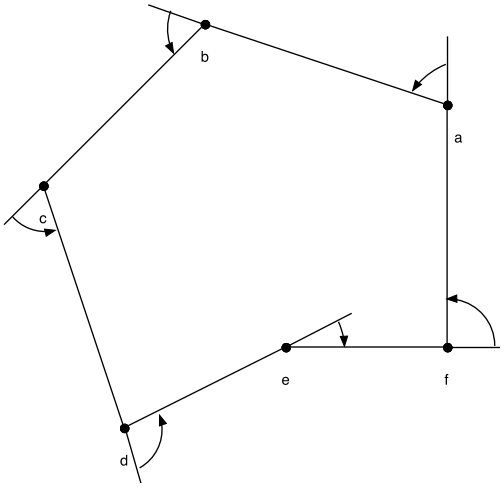

Fig. 5.2. Measuring polygon angles.

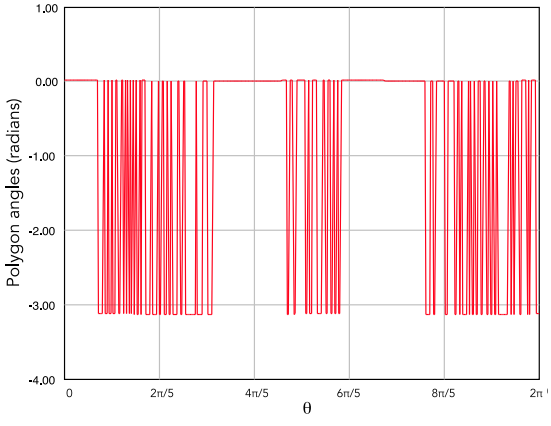

Fig. 5.3. Polygon angles (radians) of the environmental contour before smoothing.

By Proposition 3.12 it follows that if C is a known function, a convex set can always be constructed by increasing this function by a suitable positive constant. It is possible to prove that a similar effect occurs for the estimated C-function. If we add a sufficiently large positive constant to this function, the intersection points between the hyperplanes will be more spread out. As a result all the loops disappear. However, this

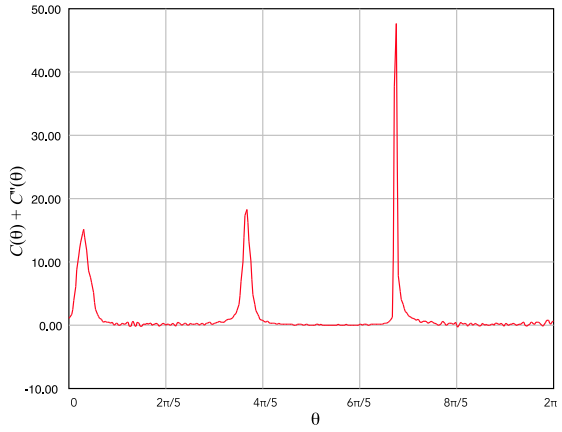

Fig. 5.4. $C(\theta) + C''(\theta)$ before smoothing.

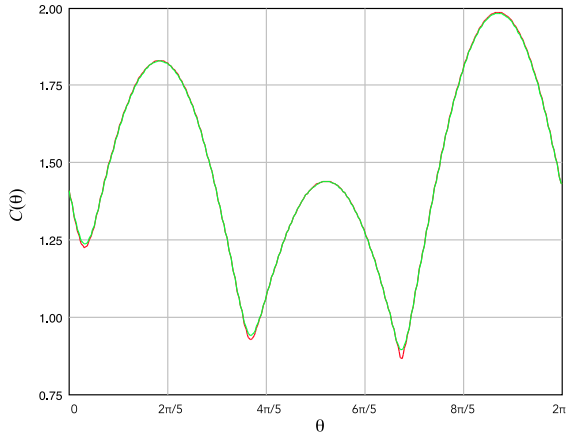

Fig. 5.5. Unsmoothed $C(\theta)$ (red curve) versus smoothed $C(\theta)$ (green curve). (For interpretation of the references to colour in this figure legend, the reader is referred to the web version of this article.)

change also inflates the contour considerably, which is usually not desirable. In the following we have chosen a different approach. By considering the plot it is evident that the issue with loops appears to be caused mostly by estimation errors. Fortunately, this problem can be remedied by applying a modest amount of smoothing. Thus, to get rid of the loops along the contour, we simply use a smoothed version of the estimated C-curve. A simple smoothing formula utilizing information from nearby points could e.g. be the following:

$$\tilde{C}(\theta_j) = \frac{\sum_{i=-w}^{+w} \omega_i C(\theta_{j+i})}{\sum_{i=-w}^{+w} \omega_i}, \quad j = 1, \dots, n,$$

where $w \geq 0$ is a suitable integer determining the number of utilized nearby points. Moreover, $\omega_{-w}, \dots, \omega_{+w}$ are suitable weights determining the influence of the nearby points. In the above formula the indices are *"looped"*, so that $\theta_{n+i} = \theta_i$, $i = 1, 2, \dots, w$, while $\theta_{1-i} = \theta_{n+1-i}$, $i = 1, 2, \dots, w$. In our calculations we have used $w = 5$ and:

$$\omega_{-i} = \omega_{+i} = (6 - i), \quad i = 0, 1, \dots, 5.$$

In Fig. 5.5 we have plotted both the unsmoothed and smoothed versions of $C(\theta)$ in the same plot. With the level of smoothing applied, the two curves are almost identical except for some areas around the local minima.

However, even this very minor adjustment has a dramatics effect on the measured angles along the contour. In Fig. 5.6 we have plotted the angles after the smoothing. These angles are indeed very different from the angles shown in Fig. 5.3.

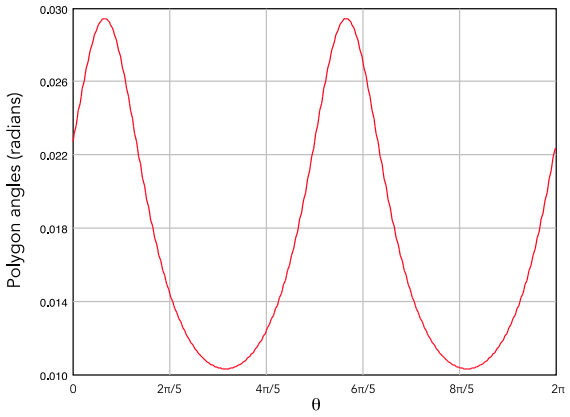

Fig. 5.6. Polygon angles (radians) of the environmental contour after smoothing.

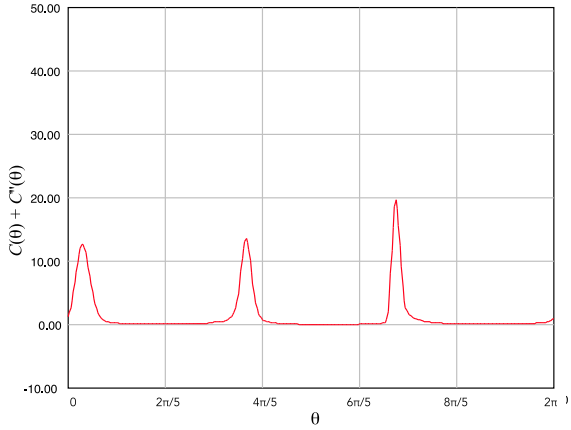

Fig. 5.7. $C(\theta) + C''(\theta)$ after smoothing.

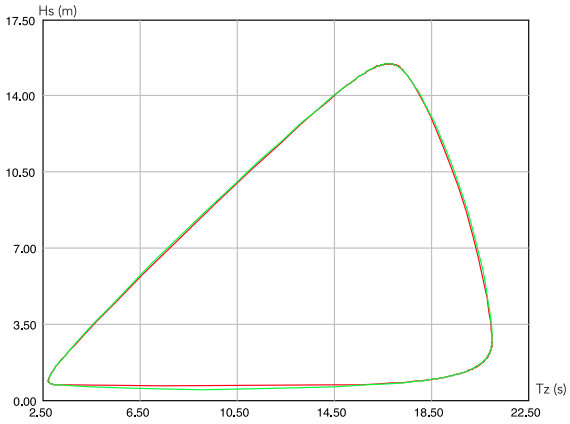

Fig. 5.8. Unsmoothed contour (red curve) versus smoothed contour (green curve). (For interpretation of the references to colour in this figure legend, the reader is referred to the web version of this article.)

In Fig. 5.7 we have plotted $C(\theta) + C''(\theta)$ after smoothing has been applied. Now all points are non-negative which by Theorem 3.11 implies that the resulting contour is convex.

Finally, in Fig. 5.8 we have plotted both the unsmoothed and smoothed contours. The two contours are apparently not very different except that the smoothed curve is somewhat more rounded. In order to avoid too strict design requirements, one wants the set $\mathcal{B}$ to be as small as possible. We observe that the set bounded by the smoothed contour is slightly larger than set bounded by the unsmoothed contour. On the other hand, by using the smoothed curve, we get a contour with a more precise exceedance probability, which after all is the most important goal.

5.1. Environmental contours and Voronoi cells

Hafver et al. (2020) has shown that the polygon given by (4.2) corresponds to the Voronoi cell of a point $\mathbf{o} = (o_x, o_y) \in \hat{\mathcal{B}}$ with respect to the function

$$s^{\mathbf{o}}(\theta) = \begin{pmatrix} o_x \\ o_y \end{pmatrix} + 2C^{\mathbf{o}}(\theta) \begin{pmatrix} \cos(\theta) \\ \sin(\theta) \end{pmatrix}, \tag{5.1}$$

where

$$C^{\mathbf{o}}(\theta) = C(\theta) - \begin{pmatrix} o_x \\ o_y \end{pmatrix} \cdot \begin{pmatrix} \cos(\theta) \\ \sin(\theta) \end{pmatrix}. \tag{5.2}$$

This means that

$$\hat{\mathcal{B}} = Vor(\mathbf{o}, S) = \left\{ \mathbf{x} \in \mathbb{R}^2 \mid \|\mathbf{x} - \mathbf{o}\| \leq \inf_{\mathbf{s} \in S} \|\mathbf{x} - \mathbf{s}\| \right\}, \tag{5.3}$$

where $S = \{s^{\mathbf{o}}(\theta) \mid \theta \in [0, 2\pi)\}$.This suggest an alternative approach to construct environmental contours, by computing the above Voronoi cell based on estimated values of $C(\theta)$. The Voronoi approach can also be used to detect hyperplanes that do not support $\mathcal{B}$, as the corresponding points in S will not be connected to $\mathbf{o}$ in the dual Delaunay triangulation. For further details see Hafver et al. (2020).

An alternative method to obtain smooth environmental contour is described in Hafver et al. (2020), where a Voronoi contour is computed based on the un-smoothed/raw $C(\theta)$ and this contour is then projected outwards on the hyperplanes $\hat{\Pi}(\theta_i)$ included in (4.2).

6. Conclusions

In the present paper we have focused on convex environmental contours, and studied various properties of such contours. By establishing a mapping between angles $\theta \in [0, 2\pi)$ and the points along the contour, we have shown that such contours can be parameterized. The mapping is valid whenever the contour set is strictly convex. A necessary condition for strict convexity is also proved. Using Monte Carlo simulations we can estimate convex environmental contours which in principle have a constant exceedance probability in all tail directions. We have shown how this procedure can be improved significantly by using importance sampling. Moreover, we have extended this methodology to cases with omission factors and mixtures. Due to numerical instabilities the contours still contain small irregularities or loops. The presence of such loops is closely related to the necessary conditions for strict convexity. By examining how this condition is violated in areas with loops, it becomes clear that the problem can be eliminated by a simple smoothing scheme. This method is demonstrated on a specific numerical example.

CRediT authorship contribution statement

Arne Bang Huseby: Discussions, Conceptualization, Writing - review & editing. **Erik Vanem:** Discussions, Conceptualization, Writing - review & editing. **Christian Agrell:** Discussions, Conceptualization, Writing - review & editing. **Andreas Hafver:** Discussions, Conceptualization, Writing - review & editing.

Declaration of competing interest

The authors declare that they have no known competing financial interests or personal relationships that could have appeared to influence the work reported in this paper.

Acknowledgements

This paper is based on research carried out with support from the Research Council of Norway (RCN) through the project *ECSADES* Environmental Contours for Safe Design of Ships and other marine structures. The authors would like to thank the anonymous referees for many valuable suggestions.

References

Baarholm, G.S., Haver, S., Økland, O.D., 2010. Combining contours of significant wave height and peak period with platform response distributions for predicting design response. Mar. Struct. 23, 147–163.

Ditlevsen, O., 2002. Stochastic model for joint wave and wind loads on offshore structures. Struct. Saf. 24, 139–163.

Hafver, A., Agrell, C., Vanem, E., 2020. Environmental contours as Voronoi cells. arXiv e-prints, arXiv:2008.13480.

Haver, S., 1987. On the joint distribution of heights and periods of sea waves. Ocean Eng. 14, 359–376.

Haver, S., Winterstein, S.R., 2009. Environmental contour lines: A method for estimating long term extremes by a short term analysis. Trans. Soc. Nav. Archit. Mar. Eng. 116, 116–127.

Huseby, A.B., Vanem, E., Natvig, B., 2013. A new approach to environmental contours for ocean engineering applications based on direct Monte Carlo simulations. Ocean Eng. 60, 124–135.

Huseby, A.B., Vanem, E., Natvig, B., 2015a. Alternative environmental contours for structural reliability analysis. Struct. Saf. 54, 32–45.

Huseby, A.B., Vanem, E., Natvig, B., 2015b. A new Monte Carlo method for environmental contour estimation. In: Nowakowski, T., Młyńczak, M., Jodejko-Pietruczuk, A., Werbińska-Wojciechowska, S. (Eds.), Safety and Reliability: Methodology and Applications, Proceedings of the European Safety and Reliability Conference. Taylor & Francis, pp. 2091–2098.

Jonathan, P., Ewans, K., Flynn, J., 2011. On the estimation of ocean engineering design contours. In: Proc. 30th International Conference on Offshore Mechanics and Arctic Engineering. pp. 1–8.

Moan, T., 2009. Development of accidental collapse limit state criteria for offshore structures. Struct. Saf. 31, 124–135.

Ottesen, T., Aarstein, J.A., 2006. The statistical boundary polygon of a two parameter stochastic process. In: Proc. 25th International Conference on Offshore Mechanics and Arctic Engineering. pp. 1–6.

Rosenblatt, M., 1952. Remarks on a multivariate transformation. Ann. Math. Stat. 23, 470–472.

Vanem, E., Huseby, A.B., 2018. Seasonal and omni-seasonal environmental contours for extreme sea states. In: Proc. 7th International Maritime Conference on Design for Safety, DfS 2018. Osaka University, Kobe, Japan, pp. 470–477.

Winterstein, S.R., 2016. Environmental Contours for Sub-Populations: Effects of Wind-Wave Direction and Cut-Out Wind Speed. Technical Report TN 2016-071, Probability-Based Engineering.

Winterstein, S.R., Ude, T.C., Cornell, C.A., Bjerager, P., Haver, S., 1993. Environmental parameters for extreme response: Inverse form with omission factors. In: Proc. 6th International Conference on Structural Safety and Reliability. pp. 551–557.